arXiv:1104.2668v1 [astro-ph.SR] 14 Apr 2011

Accepted for publication in ApJS

Radial Velocities and Pulsation Ephemerides of 11 Field RR Lyrae Stars

Bi-Qing For[1], George W. Preston[2], Christopher Sneden[1]

ABSTRACT

We present new radial velocities, improved pulsation periods and reference epochs of 11 field RR Lyrae ab-type variables: AS Vir, BS Aps, CD Vel, DT Hya, RV Oct, TY Gru, UV Oct, V1645 Sgr, WY Ant, XZ Aps and Z Mic. This study is based on high resolution spectra obtained with the echelle spectrograph of the 2.5-m du Pont telescope at Las Campanas Observatory. We obtained ~ 200 spectra per star (i.e., total of ~ 2300 spectra) distributed more or less uniformly throughout their pulsation cycles. Radial velocity curves and photometric lightcurves phased to our new ephemerides are presented for all program stars. In a subsequent paper, we will use these spectra to derive stellar atmospheric parameters and chemical compositions throughout the pulsational cycles, based purely on spectroscopic constraints.

Subject headings: stars: horizontal-branch – stars: Population II – stars: variables: RR Lyrae – techniques: radial velocities

1. Introduction

RR Lyraes (RR Lyr), named after their prototype, are old, low-mass stars that reside in the instability strip of the horizontal branch (HB). They are powerful tools in the studies of many fundamental astrophysical problems. Due to their variability and relatively high luminosity, they are easily identified even at large distances. Their small dispersion in intrinsic mean luminosity makes them good standard candles in contrast to other stellar tracers, such as M giants (Majewski et al. 2003). In addition to the distance scale, RR Lyr

---

[1] Department of Astronomy, University of Texas, Austin, TX 78712, USA; biqing@astro.as.utexas.edu

[2] Carnegie Observatories, 813 Santa Barbara Street, Pasadena, CA 91101, USA

play an important role in studying Galactic structure and formation. They are generally used to trace the spatial and kinematic distribution of the old stellar populations of the Galactic disk and halo components. For example, recent optical RR Lyrae surveys, such as QUEST (Vivas et al. 2004) and SDSS (Ivezić et al. 2004), have revealed halo substructures and dynamically young stellar streams that are associated with the formation of the outer halo.

RR Lyr are also commonly used to study the chemical evolution of the disk and halo of our Milky Way. This effort began with the pioneering low-resolution spectroscopic survey by Preston (1959), who introduced the ΔS index that describes the relation between Hydrogen and calcium K-line absorption strengths. The ΔS index varies during RR Lyrs pulsational cycle, so the standard ΔS index is defined at light minimum (i.e., near phase 0.8). High-resolution studies generally have concentrated on limited phases near minimum light, because of the relatively slow variations in photometric effective temperature that occur at these pulsation phases.

Our work in this area began as an investigation of the systematics of chemical abundances along the HB in the Galactic Halo (For & Sneden 2010). The primary objectives of that paper were to investigate any abundance anormalies in non-variable RHB and BHB stars, to derive masses of these stars and to determine the red and blue edges of the RR Lyrae instability strip. They concluded that: (1) the abundance ratios of these stars are generally consistent with those of similar-metallicity field stars in different evolutionary stages, (2) the stars possess masses of $\sim 0.5\ M_{\odot}$, and (3) the effective temperatures for the red and blue edges of HB stars in the metallicity range $-0.8 \gtrsim$ [Fe/H] $\gtrsim 2.5$ are 5900 K and 7400 K, respectively.

We are applying the analytical techniques of For & Sneden (2010) to a controlled sample of RR Lyr stars. The spectra have been gathered by GWP for his investigation of many issues in RR Lyr atmospheric dynamics, such as shocks, turbulent and Blazhko effect. This RR Lyr spectral study was also initiated partly to better understand the nature of a carbon-rich and s-process rich RRab star, TY Gru (Preston et al. 2006b). This star was identified as CS 22881−071 in the HK objective-prism survey (Beers et al. 1992) and was initially included in the study of chemical abundance of a sample metal-poor red horizontal branch stars (Preston et al. 2006a). The enrichment of carbon and n-capture species suggests that this star might have gone through binary mass transfer from a primary star during its Asymptotic Giant Branch (AGB) evolution (Preston et al. 2006b and references therein). To further investigate the abundance anomalies as seen in TY Gru and to detect the possible orbital motion caused by the relic companion of an AGB star (Preston 2011), GWP selected a sample of RRab stars with $P \sim 0.57$ day that are broadly representative of the metal-poor halo. Numerous observations at all pulsation phases provide a dataset that can be used to investigate the dependence of derived abundances on the various thermodynamic conditions that occur during pulsation cycles.

In this paper, we present radial velocities (RVs) and improved ephemerides of 11 field RRab stars. In a subsequent paper, we will report stellar parameter and chemical abundance analyses throughout the pulsational cycles (For, Sneden & Preston, in preparation). We provide the basic information on targets and describe the observations and reduction methods in §2 and §3. In §4, we present the derived radial velocities and improved ephemerides.

2. Targets and Observations

The observations were made with echelle spectrograph of the du Pont 2.5-m telescope at the Las Campanas Observatory (LCO) during 2006–2009. We used this instrument configured with the $1.5'' \times 4''$ entrance slit, which gives a resolving power of $R \equiv \lambda/\Delta\lambda \sim 27,000$ at the Mg I b lines (5180 Å). The total wavelength coverage is $3500 - 9000$ Å. Integration times ranged from a minimum value of 200 s (to insure reasonably uniform illumination of the slit by starlight) to an upper limit of 600 s (to avoid excessive blurring of the spectrum due to changing radial velocity). The values of S/N achieved by such integrations can be estimated by observations of CS 22175−034 (Preston et al. 1991), which is a star with similar colors to RR Lyrs. Spectra of this star ($V = 12.60$, $B - V = 0.37$) obtained near the zenith under typical observing conditions with an exposure time of 600 s achieved S/N$\sim$ 10 at 4050Å, S/N$\sim$ 15 at 4300Å, S/N$\sim$ 20 at 5000Å, S/N$\sim$ 30 at 6000Å and S/N$\sim$ 30 at 6600Å. Wavelength calibrations were achieved by taking Thorium-Argon comparison lamp exposures at least once per hour at each star position. Basic information about our program stars is given in Table 1.

3. Data Reduction

The raw data were bias subtracted, flat-fielded, background subtracted, then extracted to one-dimensional (1D) spectra and wavelength-calibrated by use of IRAF[1] ECHELLE package. Thorium-Argon identifications were based on the line list in the IRAF package data file (thar.dat) and the Th-Ar wavelength table[2] provided by the LCO. We paid particular attention to scattered light corrections, and in the following subsection we describe our own (non-global) approach to this problem.

---

[1] The Image Reduction and Analysis Facility, a general purpose software package for astronomical data, written and supported by the IRAF programming group of the National Optical Astronomy Observatories (NOAO) in Tucson, AZ.

3.1. Scattered Light Correction

Some of the incident photons at each wavelength are scattered into all echelle orders by optical imperfections in the optical train of the spectrograph. A generic method for making scattered light corrections is use of the IRAF apscatter task, in which the scattered light pixels are fitted by a series of 1D functions across the dispersion. The independent fits are then smoothed along the dispersion by again fitting low order functions. These fits then define the smooth scattered light surface to be subtracted from the image. Application of this method to du Pont echelle spectra is complicated by a number of considerations discussed below.

A fraction of the photons of every wavelength that passed through the $1.5'' \times 4.0''$ entrance slit were scattered into the image plane of the du Pont spectrograph by imperfect transmission/reflection at surfaces in the optical train. Longward of 6500 Å the inter-order space became too small to measure pure scattered light. To circumvent this difficulty, we obtained observations of 4 standard stars through a small $0.75'' \times 0.75''$, for which the inter-order space was more than adequate. Additional difficulties in data reduction arised due to our adopted observing procedure. Long experience at the du Pont had shown that accurate sky subtraction could not be achieved by use of light adjacent to the star image because of centering and guiding errors. If sky background is important, it must be measured by sky observations before and/or after the stellar observation, and only under good photometric conditions. For stars brighter than magnitude 13, sky was unimportant at the 1% level except near the full moon, which we avoided, so we ignored it. To save the precious time between observations that would be required to rotate the spectrograph, we made all observations with an east-west oriented slit. Furthermore, we guided with a red-sensitive detector, so that at many telescope positions significant fractions of blue-violet light did not pass through the slit due to atmospheric dispersion: the observed spectra were thus somewhat "reddened" and mimicked those of lower color temperature. In addition, this could affect the velocity difference between the red and blue lines.

To investigate such affect on our spectral line width, we calculated the velocity shifts between spectral regions at 4000–6000 Å using the followings: (1) calculate the parallactic angle for each of our stars at different 7 hour angles (from 0.01–6 hr with increment of 1 hr); (2) calculate the angle between east–west slit of Cassegrain spectrograph on equatorially–mounted telescope and direction to zenith; (3) calculate the sine of the inclination of the spectrum to the slit; (4) calculate the altitude of each star; (5) calculate differential atmospheric dispersion by linear approximate of data shown in Figure 2 of Simon (1966) for elevation 2811 m, which is close to du Pont elevation at 2200 m; (6) calculate the differential atmospheric dispersion perpendicular to the slit; (7) finally, convert angular displacement in arcsec to velocity displacement by use of scale factor 8 km s^{-1} $arcsec^{-1}$ (assuming $1.5''$ slit width projects to 12 km s^{-1}) The upper limit of 6 km s^{-1} was set for the conversion, which corresponds to an illumination centroid at the edge of the slit. During the observation, seeing and guiding errors will diminish atmospheric displacements, e.g., producing centroids nearer to aperture center. Our velocity displacement calculations over 7 hr angles of each star range from 0–2 km s^{-1}, which are small compared to intrinsic RR Lyr line width of > 20 km s^{-1}. Thus, the broadening effects of these displacements are small on individual spectra.

---

[2] http://www.lco.cl/telescopes-information/irenee-du-pont/instruments/website/echelle-spectrograph-manuals/echelle-spectrograph-manuals/atlas

To further investigate if such broadening would have any affect on the co-added spectrum, we measured the equivalent widths of several metal lines of individual spectrum and co-added spectrum of the same phase. The comparisons of measured equivalent width are consistent with an overall difference of ±3 mÅ. As such, we conclude that the equivalent widths are unaffected in these cases. However, we warn the reader that the shifts certainly contribute to systematic errors of individual radial velocities, especially for stars with large Sourthern declinations (DEC < -70). Inspecting the scatter of RV data for the stable RRab stars (WY Ant, DT Hya, CD Vel, XZ Aps, RV Oct and Zmic) of our RV curves, the errors due to blue image decentering cannot be much greater than 1 km s^{-1}.

The raw spectra of the observed standard stars were bias-subtracted and flat fielded. Then, individual spectra were combined into a single spectrum. We extracted each combined spectrum with 6 pixel aperture to two 1D spectra with one for star and one for inter-order background. Subsequently, the 1D spectra were continuum normalized with the continuum task in IRAF ECHELLE package. To obtain the contribution of scattered light in each order, we calculated the fractional contribution of the inter-order background light to the on-order starlight as a function of spectral order (or wavelength), b_λ/s_λ, for each standard star. Because a 10 pixel aperture was used to extract the spectra of our program RR Lyrs, the extracted 1D spectra are expected to contain more scattered light than the extracted scattered light frames. Thus, we applied a correction factor of 5/3 to the calculated b_λ/s_λ ratios.

In Table 2, we provide the basic information and observing log for our standard stars.

The calculated fraction as a function of spectral order for each standard star is presented in Table 3. We summarize our results in Figure 1. The success of this calibration procedure depends on the stability of the scattered light distribution produced by the spectrograph. Recalibration performed from time to time by the procedure described above has shown that the scattered light distribution has changed little, if at all, during the past two decades. We will conisder this issue more in the subsequent paper.

4. Analysis

4.1. Radial Velocities

The spectra that we used for deriving the RVs were not corrected for scattered light. It is not important for deriving the RVs but will be required for the the subsequent atmospheric analysis. We derived the RVs by use of the cross-correlation FXCOR task in IRAF, in which the individual spectra were cross-correlated against a template by fitting a Gaussian to the cross-correlation peak. We constructed the individual spectra from 13 echelle orders covering the spectral region of $4000 - 4600$ Å, which were then flattened, normalized, and stitched together with an IRAF script. In order to get strong cross-correlations that minimizes RV errors, we created a template from several spectra of CS 22874−009, a blue metal-poor radial velocity standard star (Preston & Sneden 2000), which possesses a spectrum similar to those of RR Lyr stars at most phases. The typical RV error calculated from FXCOR is ~ 0.5 km s^{-1}. We present the observed HJD midpoints, phases (see §4.2), derived RVs and their associated errors in Table 4.

4.2. Pulsation Ephemerides

A pulsation ephemeris is commonly written as HJD (max light) = T_0 + $n\times$P, where T_0 is epoch, n is the number of elapsed pulsation cycles and P is the pulsational period in days. The All Sky Automated Survey[3] (ASAS) (Pojmanski 2002) provides a starting point to obtain ephemerides for our program stars. This photometric survey has been carried out over many years at the LCO and Haleakala, Maui stations. Using the ASAS reported pulsation period and T_0, the folded lightcurves as shown on the ASAS website were slightly out of phase. This suggests that the quoted values could be improved. Here we present the methods of improving both pulsation periods and T_0 values of our program stars.

---

[3] http://www.astrouw.edu.pl/asas/

4.2.1. Pulsation Period

We improved the pulsation periods of our 10 RRab stars using the classified "grade A" V-band photometric data listed in the ASAS database. The pulsation period of TY Gru was adopted from Preston et al. (2006b) since those authors derived it by use of additional observations obtained with the LCO Swope telescope. The pulsational periods were derived using the Lomb-Scargle periodogram (Scargle 1982). We set a short period range of 0.5–0.6 day to minimize the chance of selecting spurious peaks caused by aliasing sidelobes (due to large observational gap and unevenly spaced time series data) in a different frequency domain. In addition, the pulsational period of our RRab stars is known within this range, in which a smaller time step can be set to achieve accuracy while cutting down the computing time. The advantages of this algorithm are: (1) less computing time than the lightcurve template fitting method, which requires continuous sampled data sets that are not available from the ASAS database and (2) the ability to compute Fourier Transform for unevenly spaced time series data. While we have continuous sampled RV data, we still cannot use the template fitting method because it is designed for lightcurves fitting not for RV curves of RR Lyr stars. We warn the reader that there is a caveat for this algorithm. It is optimized to identify sinusoidal-shaped periodic signal in time-series data. The lightcurves of RR Lyrae stars are non-sinusoidal.

Given that we have huge amount of photometric data, the highest peak, which represents the most probable repeating signal, in a periodogram is always more than 4σ above the mean noise level (see Figure 2). The highest peak of each periodogram is selected as the pulsational period of our program stars. We evaluated the error of the periods by comparing the periods derived from Lomb-Scargle algorithm and Box-fitting least squares method (BLS) (Kovács et al. 2002). The BLS algorithm fits the input time series with "box"-shaped function, which makes it more suitable for obtaining period for transiting lightcurve than RR Lyrs lightcurve.

In Table 5, we present the pulsation periods quoted in the ASAS catalog in column 5, the derived pulsation periods and their associated errors in column 6 and 7. The error of the period is within 0.000001–0.000007 day, which is 10 times better than the periods accuracy quoted at the ASAS website.

4.2.2. Epoch

The reference epoch (T_0) of a pulsating variable star is usually chosen to occur at visual light maximum, which closely coincides with RV minimum (see discussion by Preston 2009 and particularly Figures 4–14). Because the periodogram does not calculate an epoch, we derived values of T_0 by use of the Kwee-van Woerden method (Kwee & van Woerden 1956). This method is generally used for computing the epoch of minimum of eclipsing variables accurately but it is also suitable to determine the epoch of light maxima of variable stars. We prefer to use our RV curves for this purpose because adequate data points near the RV minima (light maxima) were available during individual cycles, in constrast to the ASAS lightcurve data that were collected over long time intervals, with few observations per cycle and relatively large scatter near light maxima.

For each star, we selected the cycles that cover the RV minima and calculated several equidistant midpoints between the rising and descending branch near the RV minima for a given cycle. Then, we fitted a linear least square equation to these midpoints, which the intersection of the straight line and the RV curve gives the T_0 of RV minima. We typically computed more than one T_0 using the above method per star to evaluate the error. Assuming the pulsational period and the first derived T_0 are accurate, we can calculate the predicted T_0 after n pulsation cycles using the defined pulsation ephemeris above. The predicted T_0 should be close to the second derived T_0. The difference between the predicted and the derived value provides an estimate for the error. Due to the possibility of period change for the Blazhko RRab stars, several epochs were determined and used for folding their RV curves.

In Figure 3, we show the schematic diagram that determines the times of RV minima of our asymmetric RV curves. We refer the reader to Kwee & van Woerden (1956) for the mathematical description of the method (for symmetric lightcurve only). In Table 5, we summarize the ephemerides of 11 field RRab stars. We tabulate epochs for the particular RV minima used to derive them. The table also gives the range of data in HJD that are associated with the corresponding T_0 and pulsational periods. We present the folded RV curves and ASAS lightcurves with our derived ephemerides in top and bottom panels of Figure 4–14. The figures are arranged by ascending right ascension.

B.-Q. For acknowledges travel assistance from a SigmaXi grant-in-aid. This research was supported by U.S. National Science Foundation grants AST-0908978.

REFERENCES

Beers, T. C., Preston, G. W., & Shectman, S. A. 1992, AJ, 103, 1987

For, B., & Sneden, C. 2010, AJ, 140, 1694

Ivezić, Ž., et al. 2004, in Astronomical Society of the Pacific Conference Series, Vol. 327, Satellites and Tidal Streams, ed. F. Prada, D. Martinez Delgado, & T. J. Mahoney, 104–+

Kovács, G., Zucker, S., & Mazeh, T. 2002, A&A, 391, 369

Kwee, K. K., & van Woerden, H. 1956, Bull. Astron. Inst. Netherlands, 12, 327

Majewski, S. R., Skrutskie, M. F., Weinberg, M. D., & Ostheimer, J. C. 2003, ApJ, 599, 1082

Pojmanski, G. 2002, Acta Astron., 52, 397

Preston, G. W. 1959, ApJ, 130, 507

—. 2009, A&A, 507, 1621

—. 2011, AJ, 141, 6

Preston, G. W., Shectman, S. A., & Beers, T. C. 1991, ApJS, 76, 1001

Preston, G. W., & Sneden, C. 2000, AJ, 120, 1014

Preston, G. W., Sneden, C., Thompson, I. B., Shectman, S. A., & Burley, G. S. 2006a, AJ, 132, 85

Preston, G. W., Thompson, I. B., Sneden, C., Stachowski, G., & Shectman, S. A. 2006b, AJ, 132, 1714

Scargle, J. D. 1982, ApJ, 263, 835

Simon, G. W. 1966, AJ, 71, 190

Szczygieł, D. M., & Fabrycky, D. C. 2007, MNRAS, 377, 1263

Vivas, A. K., et al. 2004, AJ, 127, 1158

This preprint was prepared with the AAS LaTeX macros v5.2.

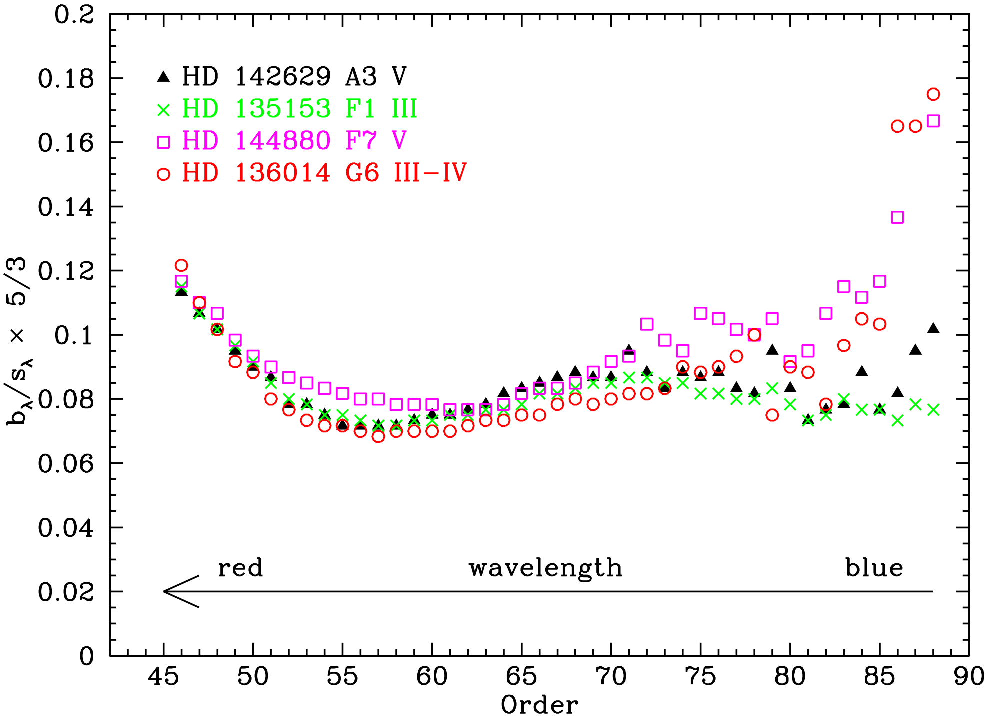

Fig. 1.— Fractional contribution of the inter-order background light to the on-order starlight as a function of spectral order (wavelength), b_λ/s_λ, for each standard star. Wavelength decreases with increasing order.

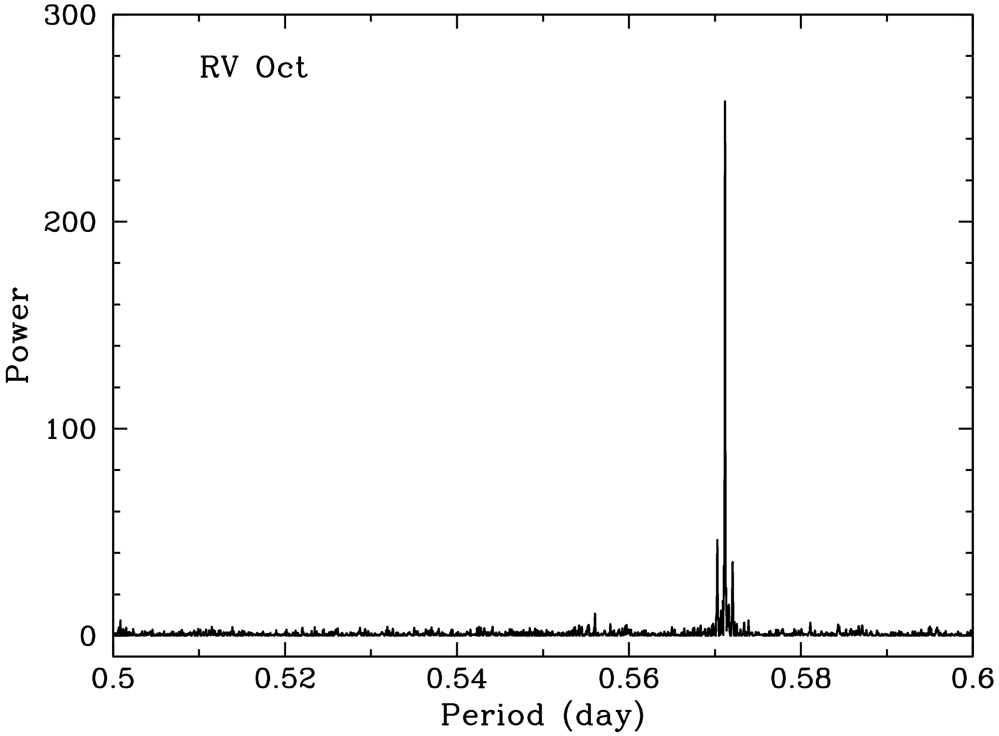

Fig. 2.— An example of typical periodogram used for searching the pulsational period. The sidelobes that caused by the large observing gap is clearly seen in the periodogram. The highest peak defines the pulsational period of RV Oct.

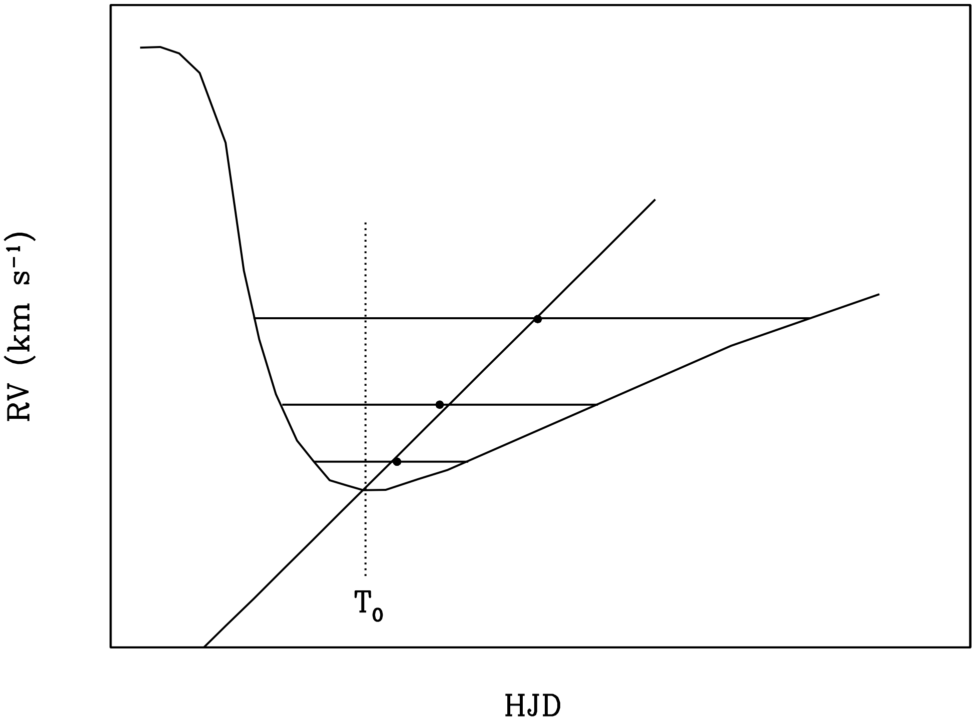

Fig. 3.— A schematic diagram that shows the typical radial velocity curve near minima (or equivalent to light maxima) of a RRab variable star. It also shows the Kwee-van Woerden method (Kwee & van Woerden 1956) that we applied to determine the epochs of our RR Lyrae stars.

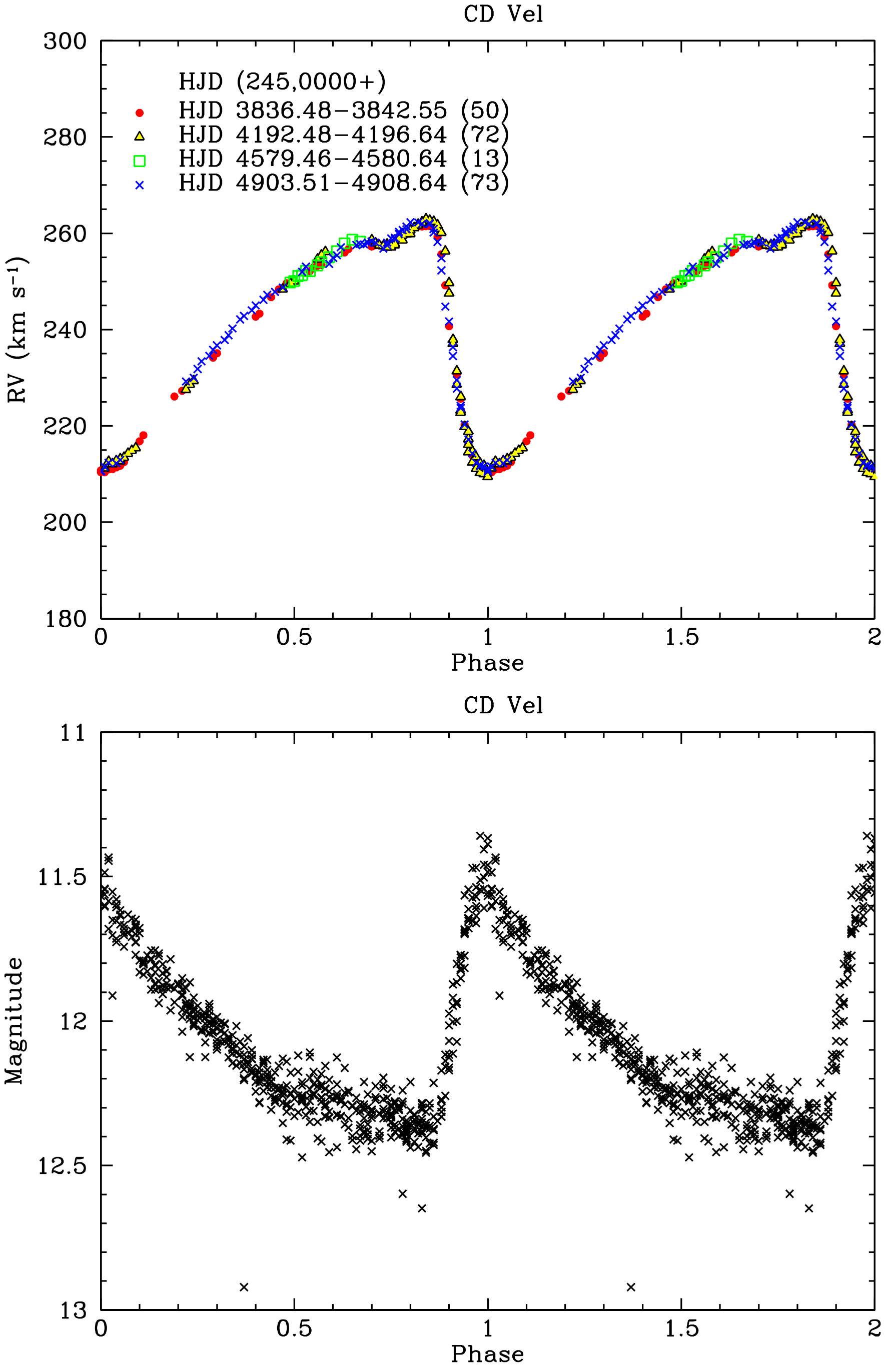

Fig. 4.— Folded radial velocity curve and lightcurve of CD Vel by using our derived ephemeris for this star (Table 5). Top panel: Radial velocity vs pulsational phase for all of our spectra. The different symbols and colors represent different times of observations in HJD. The total numbers of observed spectra per cycle are listed in the parentheses. Bottom panel: The ASAS photometric lightcurve vs pulsational phase. The scatter of data points at a given phase for CD Vel and for the other program stars is highly related to the mean apparent brightness of the observed star.

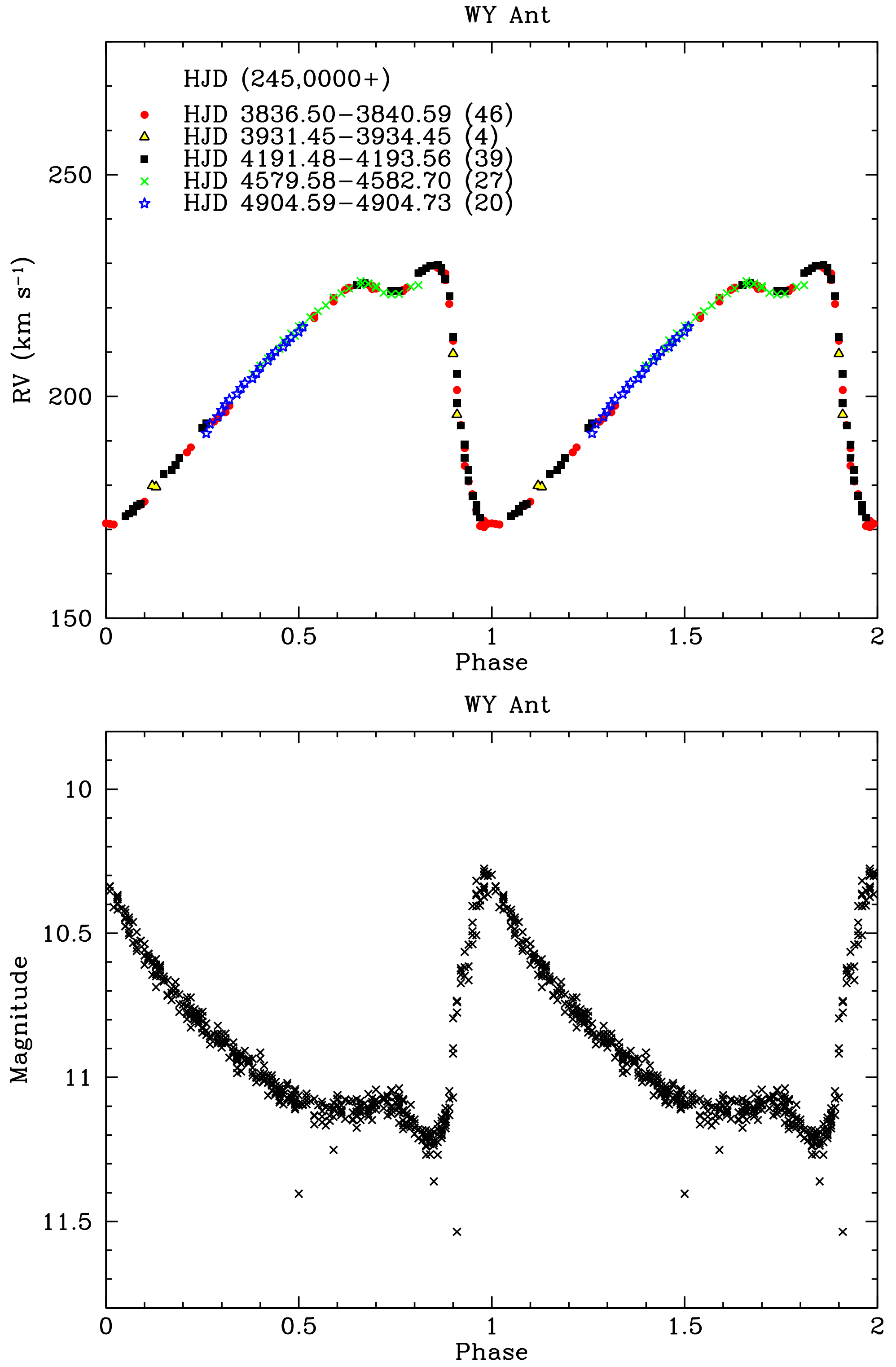

Fig. 5.— Same as Figure 4.

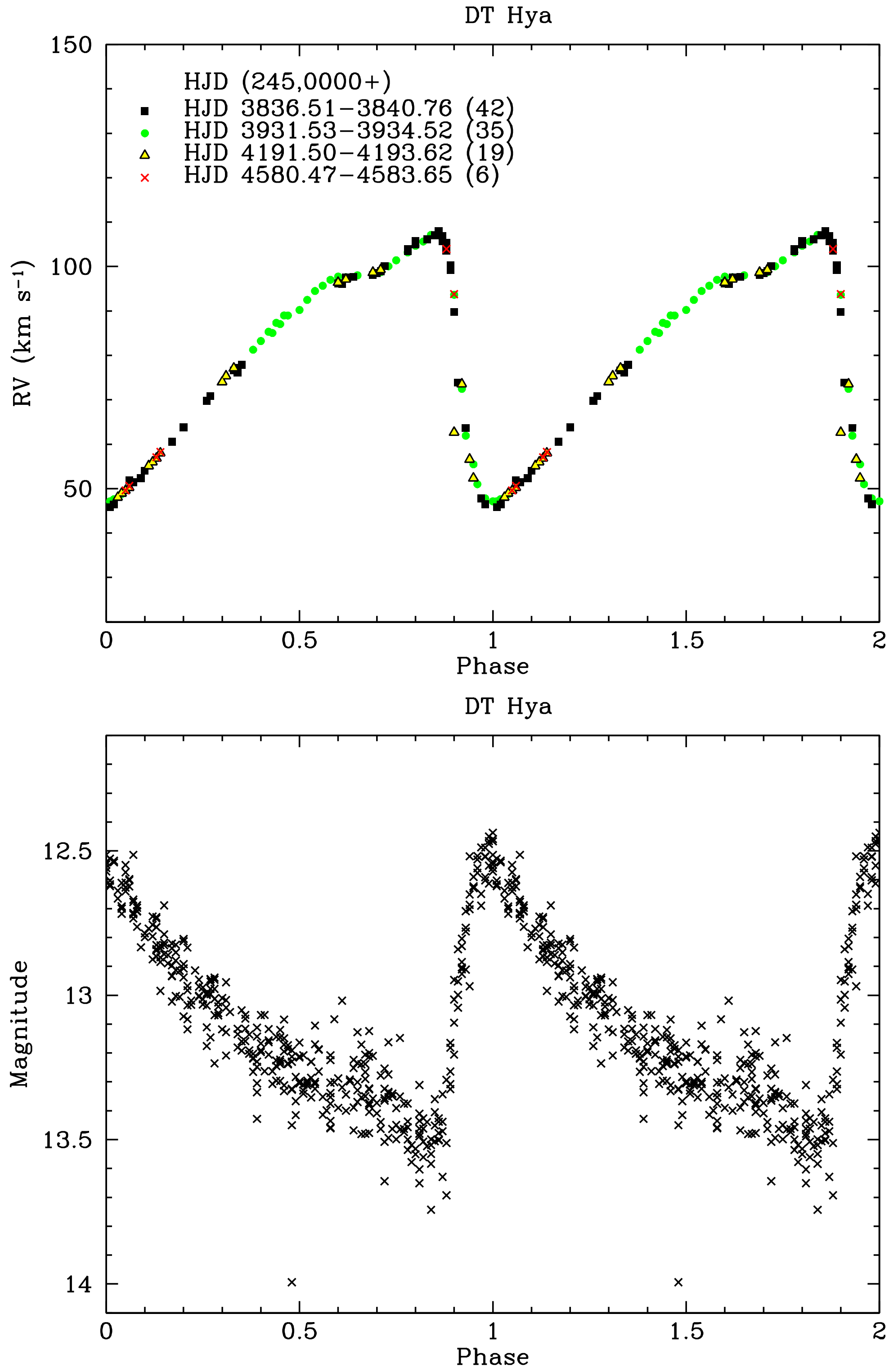

Fig. 6.— Same as Figure 4.

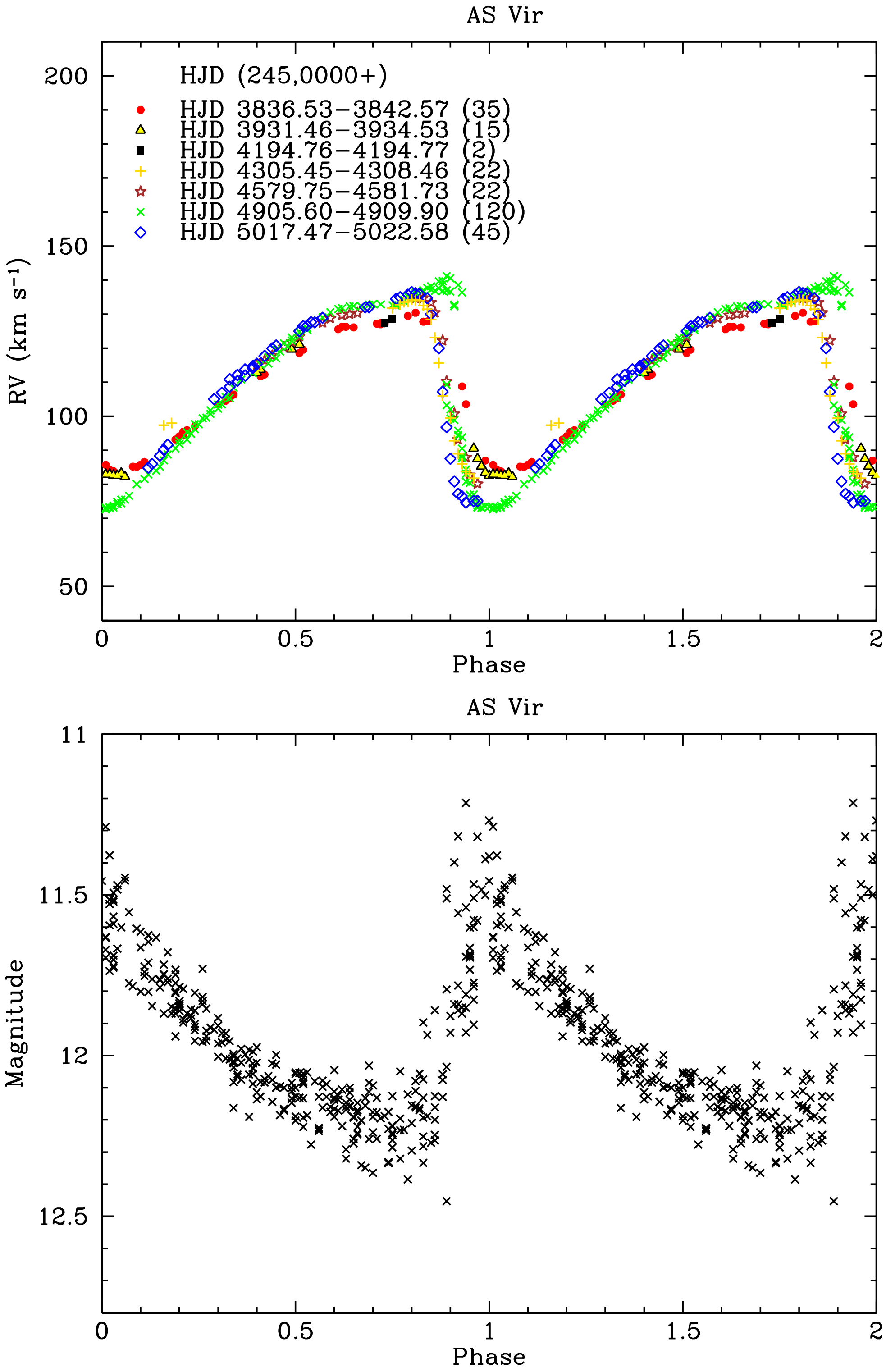

Fig. 7.— Same as Figure 4.

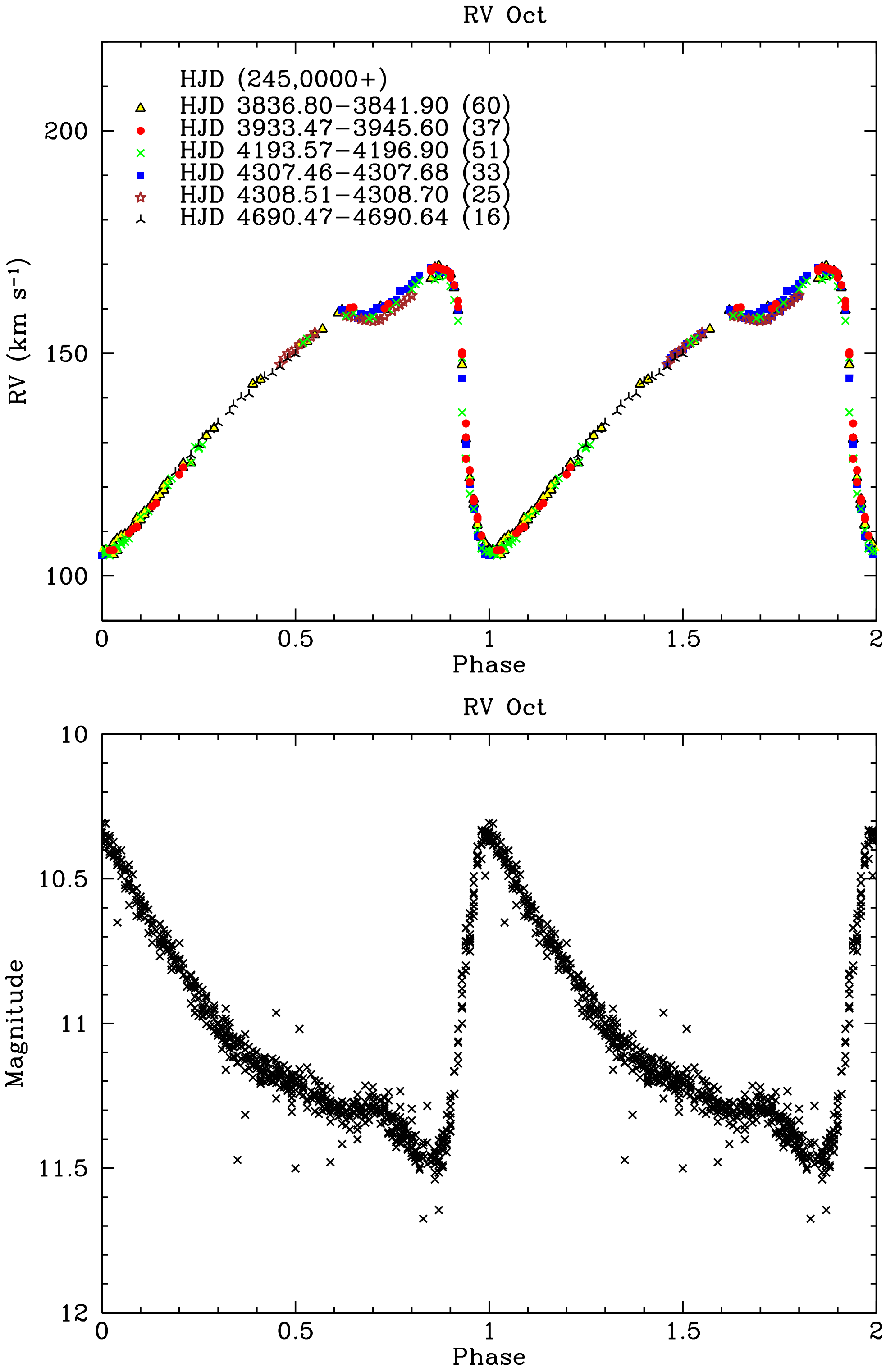

Fig. 8.— Same as Figure 4.

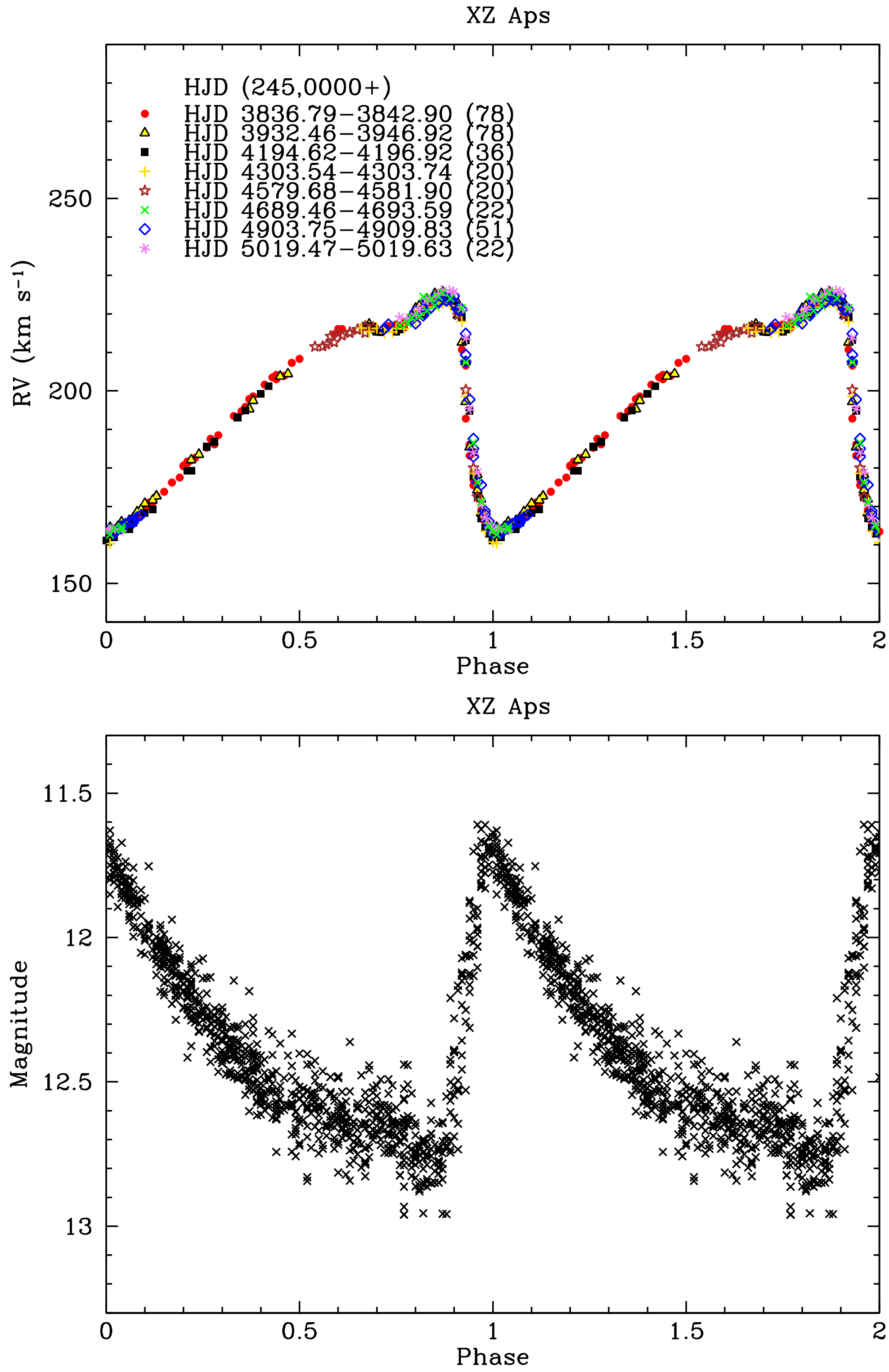

Fig. 9.— Same as Figure 4.

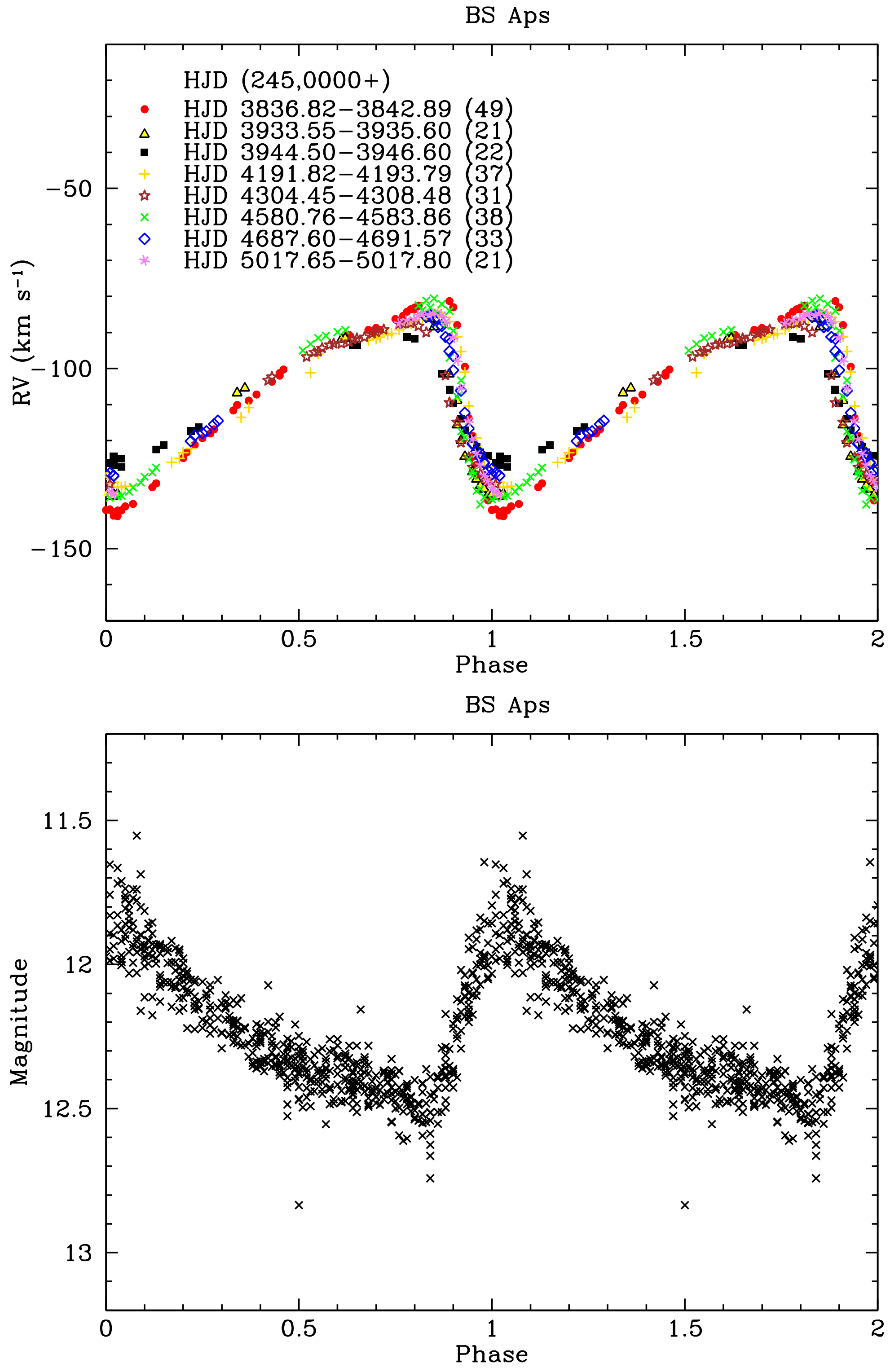

Fig. 10.— Same as Figure 4.

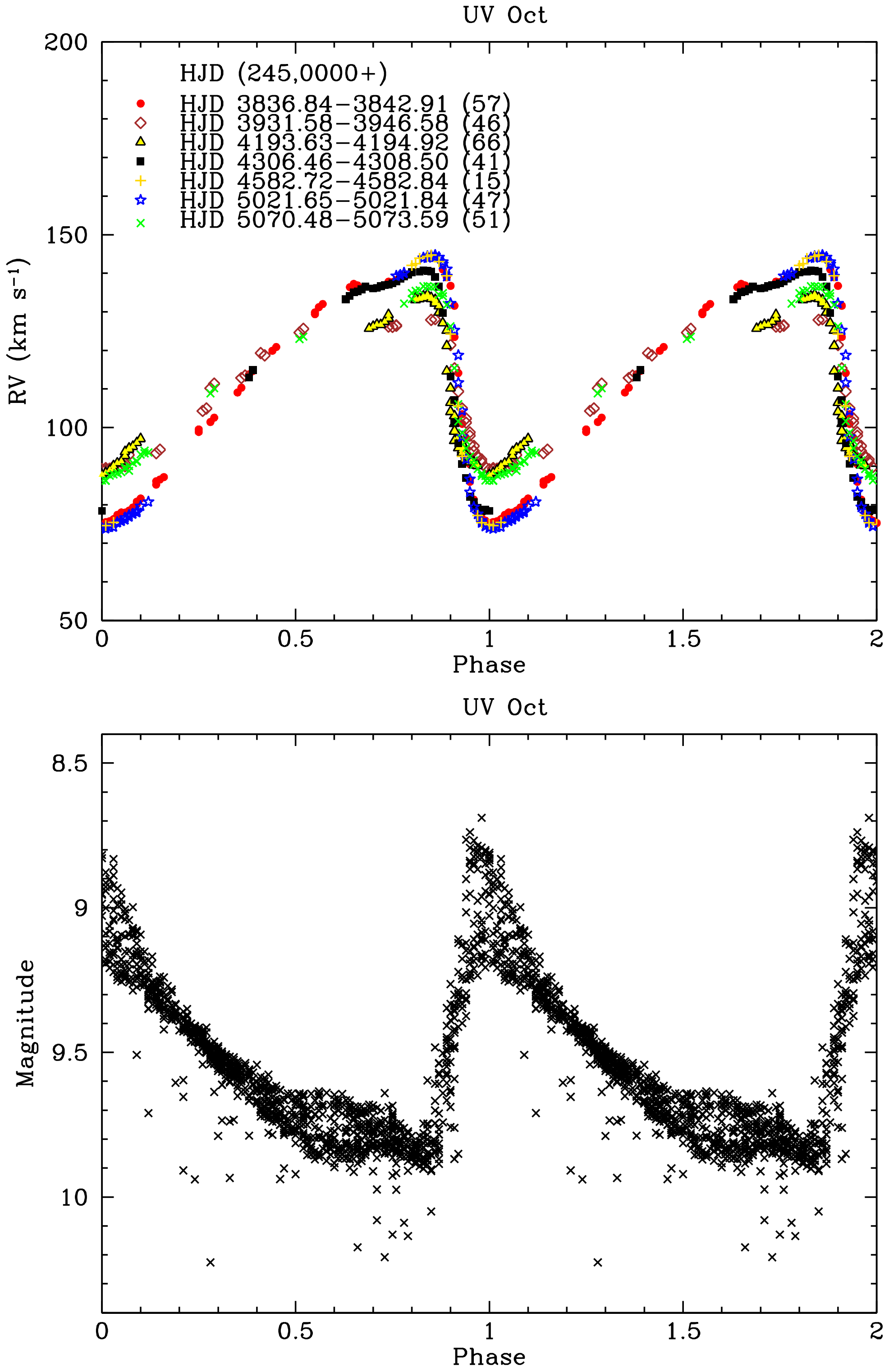

Fig. 11.— Same as Figure 4.

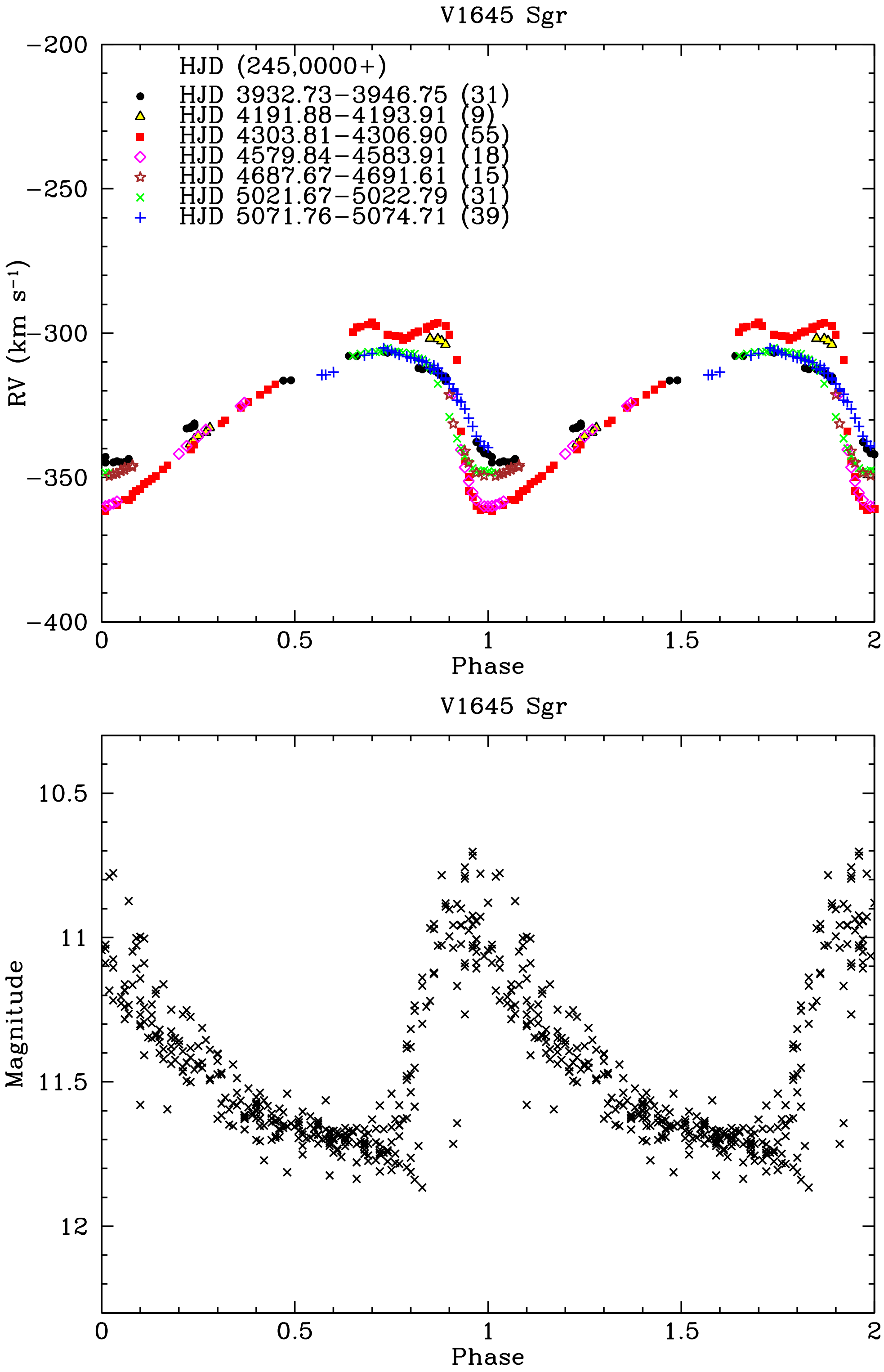

Fig. 12.— Same as Figure 4.

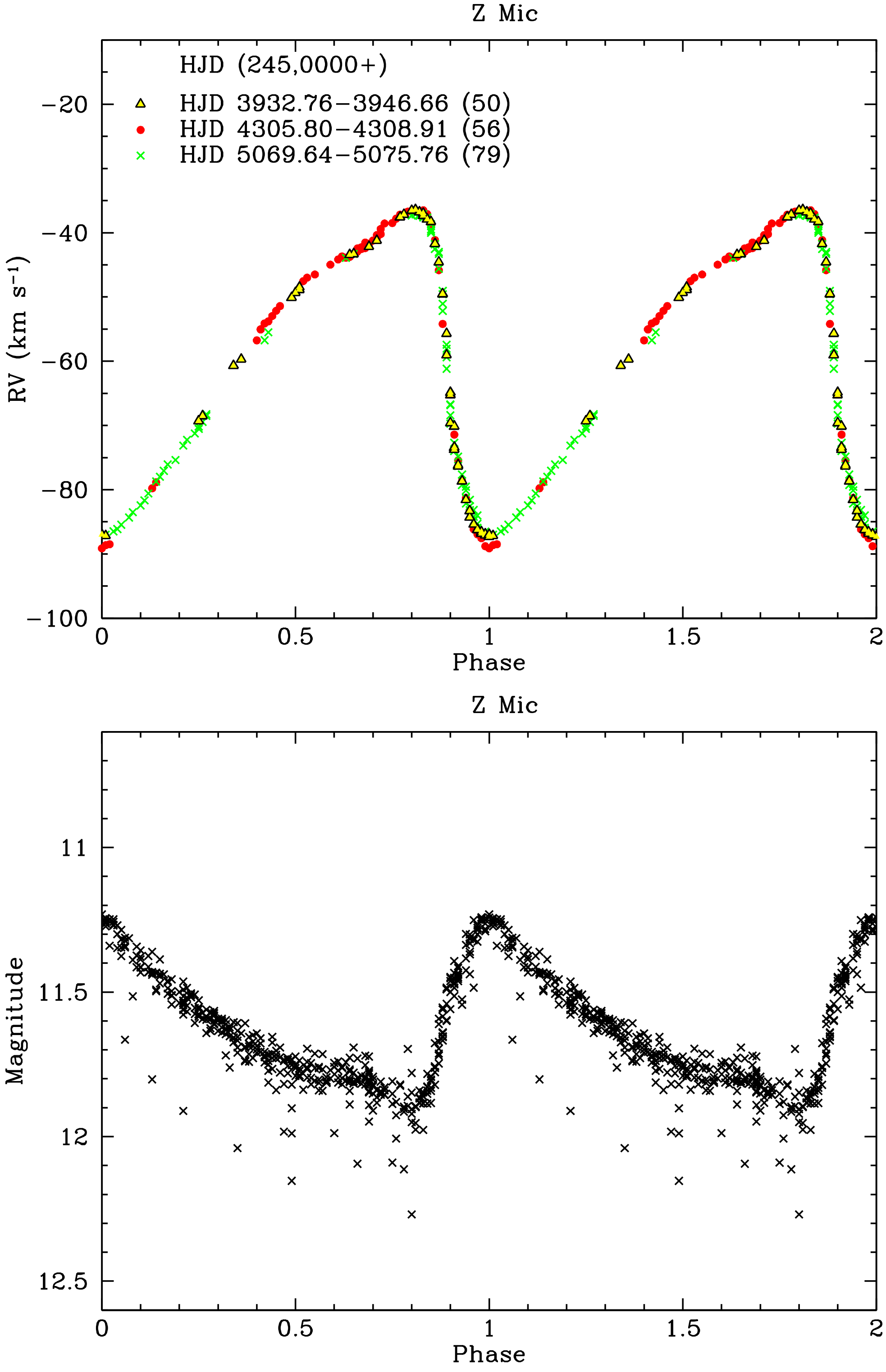

Fig. 13.— Same as Figure 4.

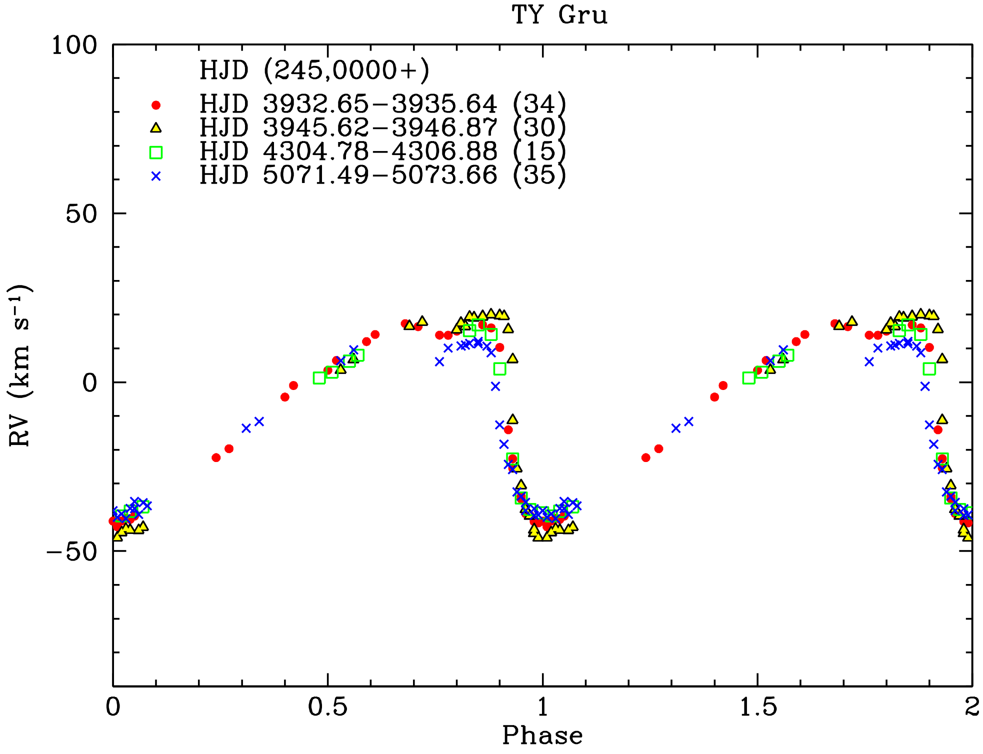

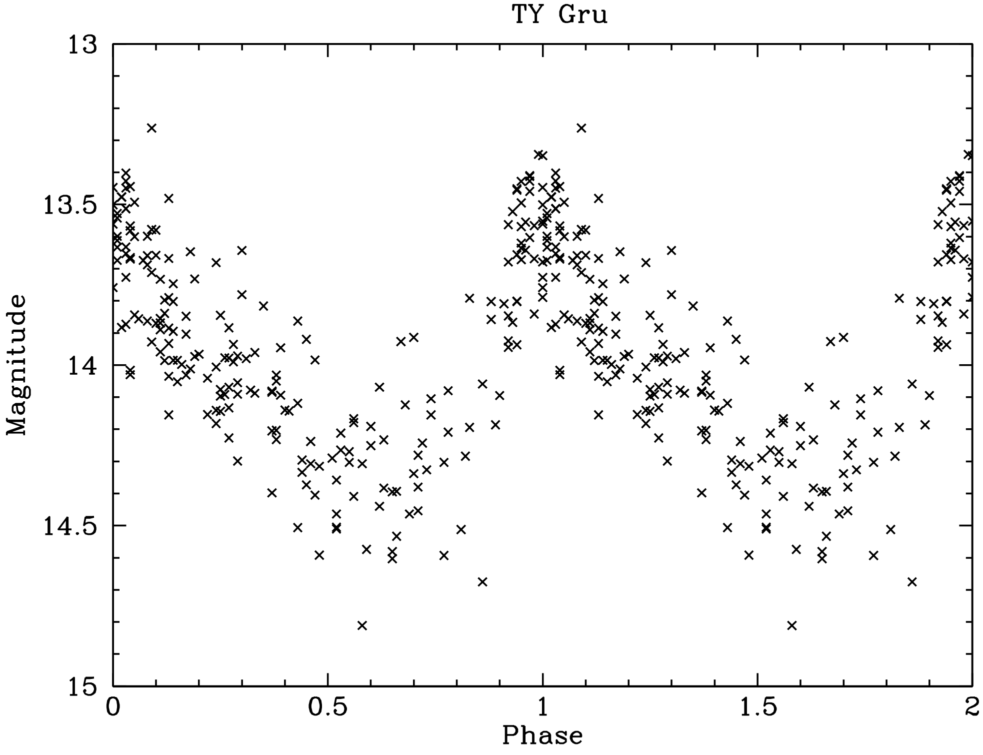

Fig. 14.— Same as Figure 4.

Table 1. Program stars.

Star	R.A.(J2000) (hr m s)	Decl.(J2000) (° ′ ″)	$V_{\rm max}$[a] (mag)	$V_{\rm amp}$[a] (mag)	Note
CD Vel	09 44 38.24	−45 52 37.2	11.66	0.87	Blazhko[c]
WY Ant	10 16 04.95	−29 43 42.4	10.37	0.85	···
DT Hya	11 54 00.18	−31 15 40.0	12.53	0.98	···
AS Vir	12 52 45.86	−10 15 36.4	11.66	0.72	Blazhko
RV Oct	13 46 31.75	−84 24 06.4	10.53	1.13	Blazhko
XZ Aps	14 52 05.43	−79 40 46.6	11.94	1.1	···
BS Aps	16 20 51.51	−71 40 15.8	11.9	0.68	Blazhko
UV Oct	16 32 25.53	−83 54 10.5	9.19	0.82	Blazhko
V1645 Sgr	20 20 44.47	−41 07 05.7	10.99	0.84	Blazhko
Z Mic	21 16 22.71	−30 17 03.1	11.32	0.64	Blazhko
TY Gru	22 16 39.42	−39 56 18.0	13.6[d]	0.9[d]	Blazhko

[a] Maximum light in V magnitude from ASAS.

[b] Pulsational amplitude in V-band from ASAS.

[c] Szczygieł & Fabrycky (2007).

[d] Values extracted from Preston et al. (2006b).

Table 2. Basic Information and Observing Log of Standard Stars

Star	Spectral Type	R.A. (h m s)	Decl. (° ′ ″)	V (mag)	UT Date	N_{exp}
HD 142629	A3 V	15 56 53.498	−33 57 58.08	5.095	08,09 Aug 2008	2,2
HD 135153	F1 III	15 14 37.319	−31 31 08.84	4.924	09 Aug 2008	3
HD 144880	F7 V	16 09 11.123	−32 06 01.20	7.45	09 Aug 2008	5
HD 136014	G6 III-IV	15 19 31.720	−37 05 49.78	6.189	09 Aug 2008	4

Table 3. Mean background fractions b_λ/s_λ for Du Pont echelle spectrograph.

		HD 142629		HD 135153		HD 144880		HD 136014	
Order	λ_c[a]	Mean	Mean×5/3	Mean	Mean×5/3	Mean	Mean×5/3	Mean	Mean×5/3
46	7575	0.068	0.113	0.069	0.115	0.070	0.117	0.073	0.122
47	7415	0.064	0.107	0.064	0.107	0.066	0.110	0.066	0.110
48	7260	0.061	0.102	0.061	0.102	0.064	0.107	0.061	0.102
49	7108	0.057	0.095	0.058	0.097	0.059	0.098	0.055	0.092
50	6962	0.054	0.090	0.055	0.092	0.056	0.093	0.053	0.088
51	6825	0.052	0.087	0.051	0.085	0.054	0.090	0.048	0.081
52	6688	0.047	0.078	0.048	0.080	0.052	0.087	0.046	0.077
53	6560	0.047	0.078	0.047	0.078	0.051	0.085	0.044	0.073
54	6435	0.045	0.075	0.045	0.075	0.050	0.083	0.043	0.072
55	6315	0.043	0.072	0.045	0.075	0.049	0.082	0.043	0.071
56	6202	0.043	0.072	0.044	0.073	0.048	0.080	0.042	0.070
57	6092	0.043	0.072	0.043	0.072	0.048	0.080	0.041	0.069
58	5987	0.043	0.072	0.043	0.072	0.047	0.078	0.042	0.069
59	5880	0.044	0.073	0.044	0.073	0.047	0.078	0.042	0.070
60	5780	0.045	0.075	0.044	0.073	0.047	0.078	0.042	0.071
61	5686	0.045	0.075	0.045	0.075	0.046	0.077	0.042	0.071
62	5592	0.046	0.077	0.045	0.075	0.046	0.077	0.043	0.071
63	5502	0.047	0.078	0.046	0.077	0.046	0.077	0.044	0.073
64	5413	0.049	0.082	0.046	0.077	0.047	0.078	0.044	0.073
65	5330	0.050	0.083	0.047	0.078	0.049	0.082	0.045	0.074
66	5250	0.051	0.085	0.049	0.082	0.050	0.083	0.045	0.076
67	5170	0.052	0.087	0.049	0.082	0.050	0.083	0.047	0.078
68	5090	0.053	0.088	0.050	0.083	0.051	0.085	0.048	0.080
69	5017	0.052	0.087	0.051	0.085	0.053	0.088	0.047	0.079
70	4945	0.052	0.087	0.051	0.085	0.055	0.092	0.048	0.080
71	4870	0.057	0.095	0.052	0.087	0.056	0.093	0.049	0.082
72	4805	0.053	0.088	0.052	0.087	0.062	0.103	0.049	0.082
73	4740	0.050	0.083	0.051	0.085	0.059	0.098	0.050	0.084
74	4672	0.053	0.088	0.051	0.085	0.057	0.095	0.054	0.090
75	4610	0.052	0.087	0.049	0.082	0.064	0.107	0.053	0.089
76	4548	0.053	0.088	0.049	0.082	0.063	0.105	0.054	0.090
77	4490	0.050	0.083	0.048	0.080	0.061	0.102	0.056	0.093
78	4430	0.049	0.082	0.048	0.080	0.060	0.100	0.060	0.100
79	4375	0.057	0.095	0.050	0.083	0.063	0.105	0.045	0.074
80	4320	0.050	0.083	0.047	0.078	0.055	0.092	0.054	0.090
81	4265	0.044	0.073	0.044	0.073	0.057	0.095	0.053	0.088
82	4210	0.046	0.077	0.045	0.075	0.064	0.107	0.047	0.078
83	4160	0.047	0.078	0.048	0.080	0.069	0.115	0.058	0.097
84	4110	0.053	0.088	0.046	0.077	0.067	0.112	0.063	0.105
85	4060	0.046	0.077	0.046	0.077	0.070	0.117	0.062	0.104
86	4012	0.049	0.082	0.044	0.073	0.082	0.137	0.099	0.166
87	3966	0.057	0.095	0.047	0.078	0.123	0.205	0.099	0.165
88	3920	0.061	0.102	0.046	0.077	0.100	0.167	0.105	0.175

[a] Central wavelength of the order.

Table 4. Radial Velocities

Star	HJD at midpoint (2450000+)	Phase (ϕ)	RV (km s^{-1})	err (km s^{-1})
CD Vel	3836.48565	0.00	210.76	0.50
	3836.49453	0.02	210.97	0.48
	3836.54295	0.10	216.80	0.35
	3836.54928	0.11	218.06	0.35
	.	.	.	.
	.	.	.	.
	.	.	.	.

Note. — Table 4 is published in its entirety in the electronic edition of the *Astrophysical Journal Supplement Series*. A portion is shown here for guidance regarding its form and content.

Table 5. Ephemerides of our program stars

Star	Data used (HJD 2450000+)	T_0[a] (HJD 2450000+)	err (HJD 2450000+)	Period[b] (day)	Period (day)	error (day)
CD Vel	all	3837.632	0.0003	0.57351	0.573510	0.000003
WY Ant	all	4191.685	0.0097	0.57434	0.574344	0.000002
DT Hya	all	4583.637	0.0089	0.56797	0.567978	0.000001
AS Vir	all	4907.709	0.0098	0.553439	0.553412	0.000002
RV Oct	all	3841.602	0.0016	0.571184	0.571170	0.000002
XZ Aps	all	3842.735	0.0052	0.5873	0.587264	0.000002
BS Aps	all	4583.785	0.0045	0.582577	0.582561	0.000007
UV Oct	3836.843842.91, 4306.465021.84	3837.875	0.0072	0.542561	0.542578	0.000003
	3931.584194.92, 5070.485073.59	5070.605	0.0072	···	···	···
V1645 Sgr	4191.894306.90	4306.775	0.0150	0.552979	0.552948	0.000005
	4579.854583.91	4579.895	0.0150	···	···	···
	3932.733946.75, 4687.665074.71	4687.703	0.0170	···	···	···
Z Mic	all	5075.606	0.0015	0.58693	0.586926	0.000001
TY Gru	3933.793935.65, 5071.50–5073.66	3933.785	0.0120	···	0.570065	0.000005
	3945.634306.89	4304.885	0.0120	···	···	···

[a] Epoch at time of light maxima or radial velocity minima.

[b] isted in ASAS catalog.